SI

ELECTRONIC SUPPLEMENTARY INFORMATION

Tetra-, tetradeca- and octadecametallic clusters of Mn

Eleftheria Agapaki,[a] Angelos B. Canaj,[a] Gary S. Nichol[a] and Euan K. Brechin*[a]

[a]EaStCHEM School of Chemistry, The University of Edinburgh, David Brewster Road, Edinburgh, EH9 3FJ, Scotland, UK. Email: ebrechin@ed.ac.uk
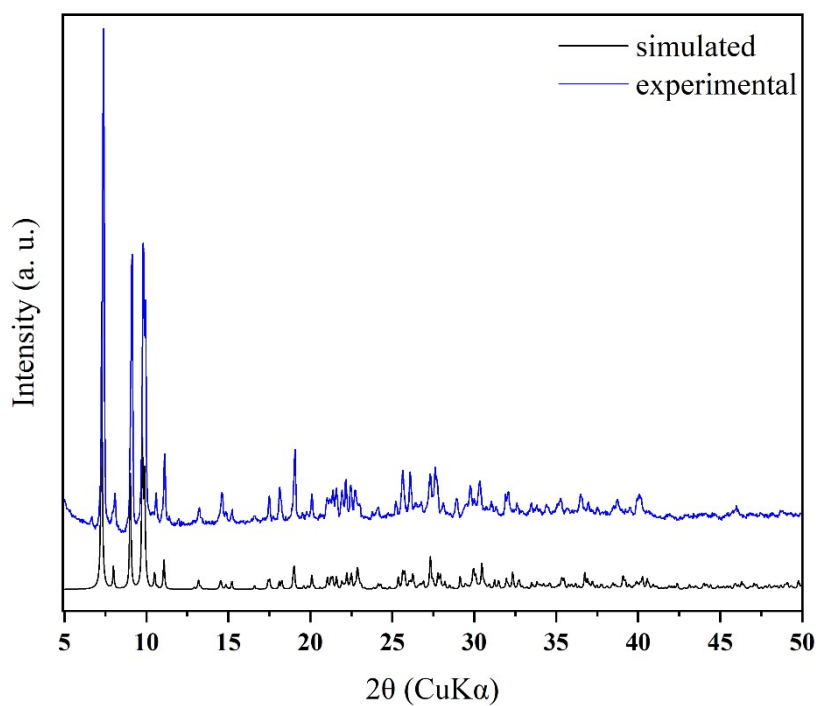
1. Characterization

Fig. S1. Powder X-ray data for **1**. The blue and black lines are the experimental and simulated data, respectively.
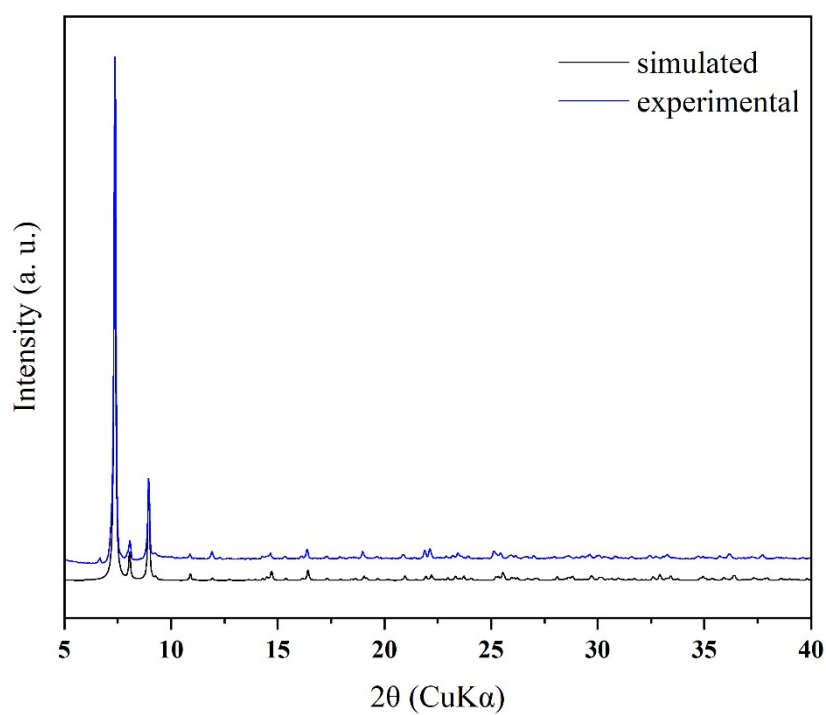

Fig. S2. Powder X-ray data for **2**. The blue and black lines are the experimental and simulated data, respectively.
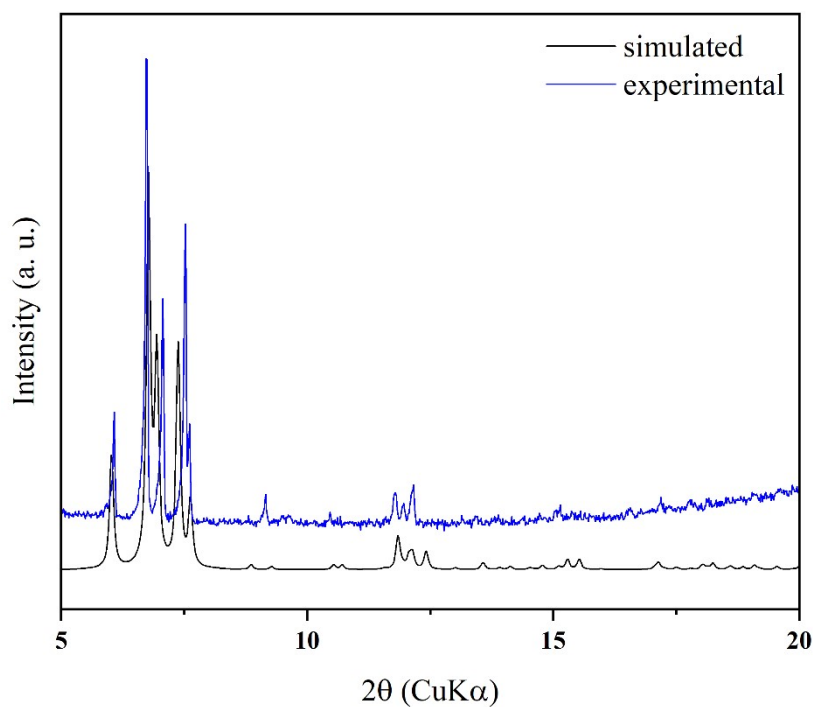
Fig. S3. Powder X-ray data for **3**. The blue and black lines are the experimental and simulated data, respectively.

Table S1. Bond valence sum calculation for the metal ions in compound **1**-**3**.

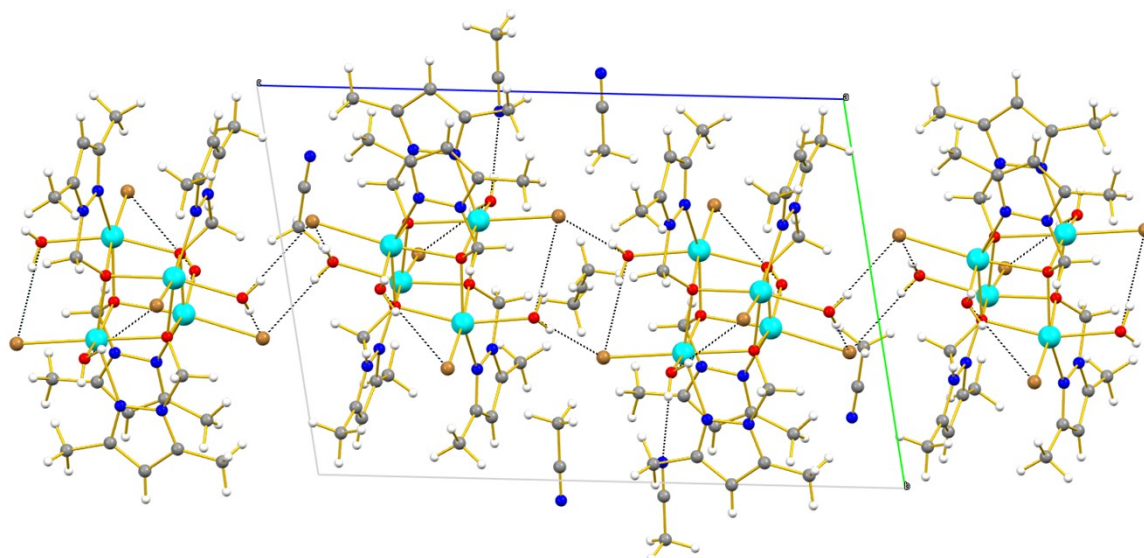| Compound 1	Mn^{II}	Mn^{III}	Mn^{IV}
Mn1	1.94	2.00	1.98
Mn2	1.91	1.97	1.95
Mn3	1.96	2.02	2.00
Mn4	1.91	1.98	1.96
Compound 2	**Mn^{II}**	**Mn^{III}**	**Mn^{IV}**
Mn1	1.85	1.93	1.89
Mn2	1.89	1.91	1.84
Mn3	1.95	1.98	1.90
Mn4	3.17	3.21	3.08
Compound 3	**Mn^{II}**	**Mn^{III}**	**Mn^{IV}**
Mn1	3.17	3.21	3.08
Mn2	3.12	3.16	3.03
Mn3	3.24	3.29	3.15
Mn4	3.06	3.19	3.13
Mn5	1.89	1.96	1.92
Mn6	3.19	3.23	3.10
Mn7	1.82	1.88	1.84
Mn8	3.03	3.07	2.95
Mn9	3.18	3.22	3.09

Fig. S4. Packing of the clusters of **1** in the extended structure viewed down the *a*-axis of the unit cell. H-bonds are highlighted with thin black dotted lines. Colour code: Mn^{II} = light blue, C = grey, O = red, N = dark blue, Br = brown. H = white.
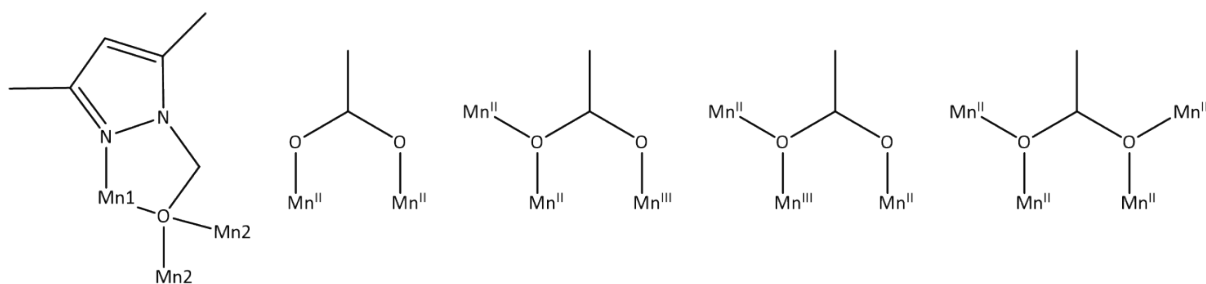

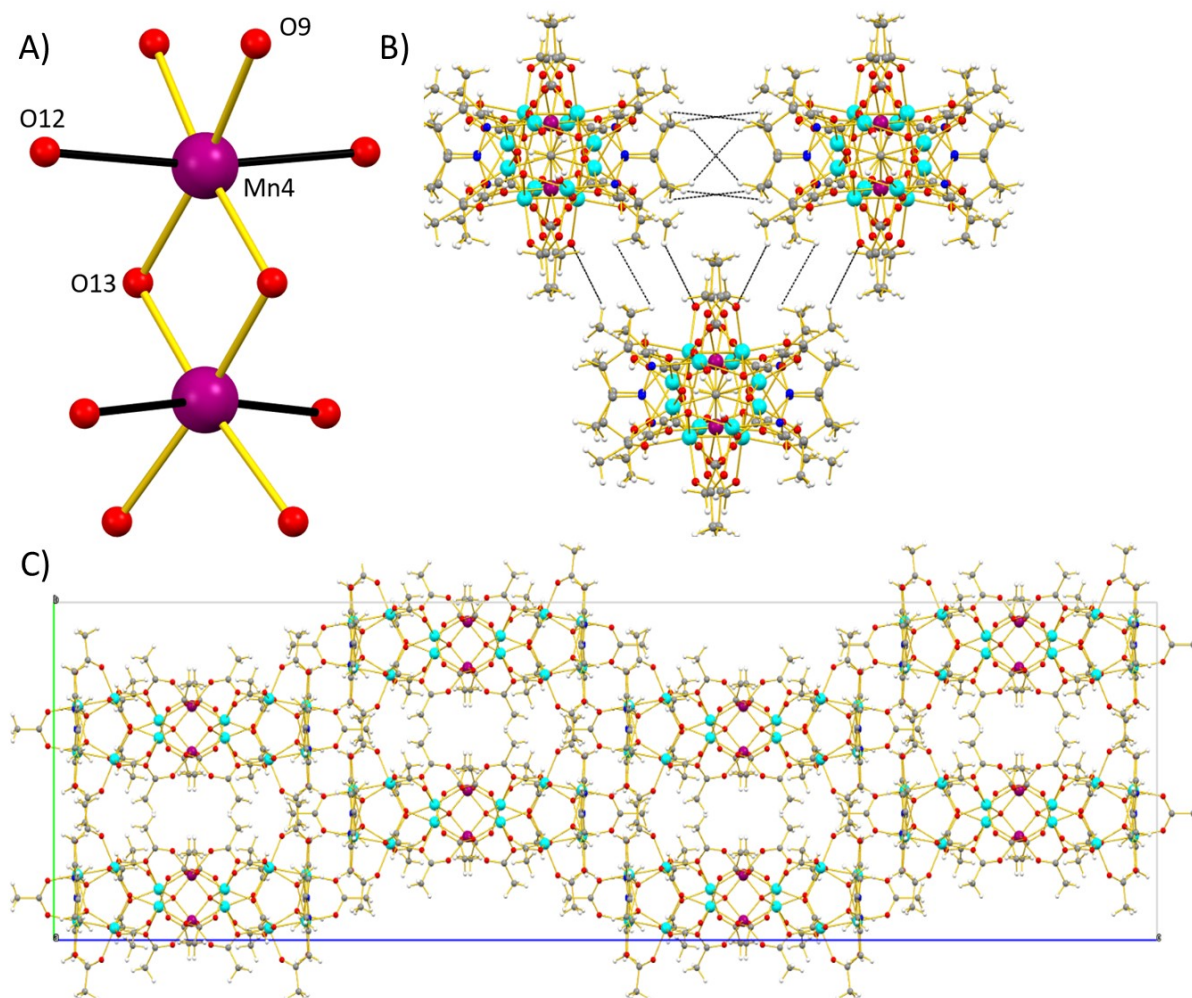**Fig. S5**. The bridging modes displayed by L^1 and the OAc ligands in **2**.

Fig. S6. A) The central [Mn$^{III}_2$] unit in **2**, highlighting the co-parallel Jahn-Teller axes in black. B) View of the close contacts (thin black dotted lines) between clusters of **2**, viewed down the *c*-axis. C) Packing of the clusters of **2** in a brickwork-like motif in the extended structure, viewed down the *a*-axis (top).
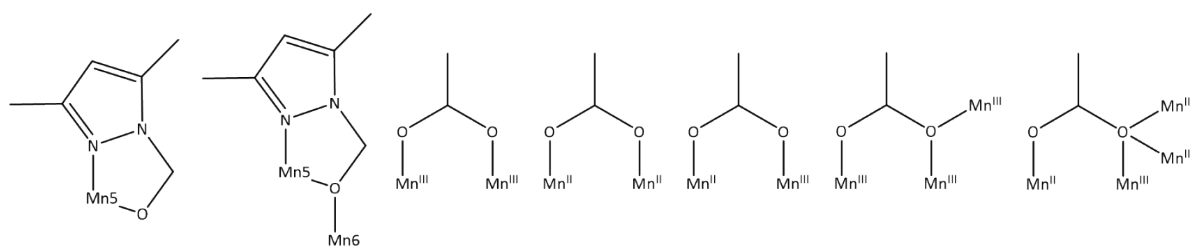

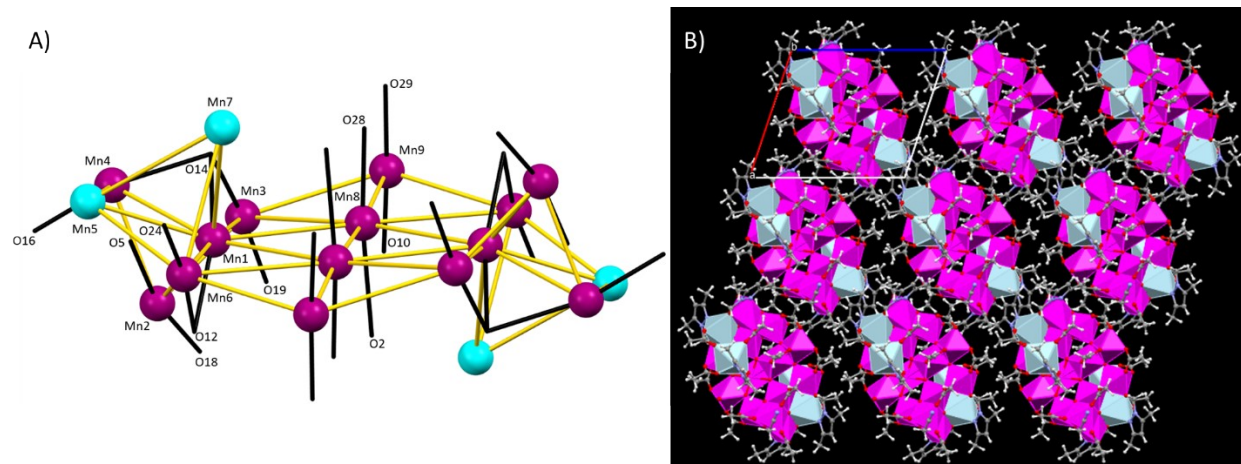**Fig. S7**. Bridging modes displayed by the HL^1, L^1 and OAc ligands in **3**.

Fig. S8. A) The metal core of 3 highlighting the positions of the Jahn-Teller axes in black. B) Packing of **3** in the extended structure viewed down the *b*-axis.
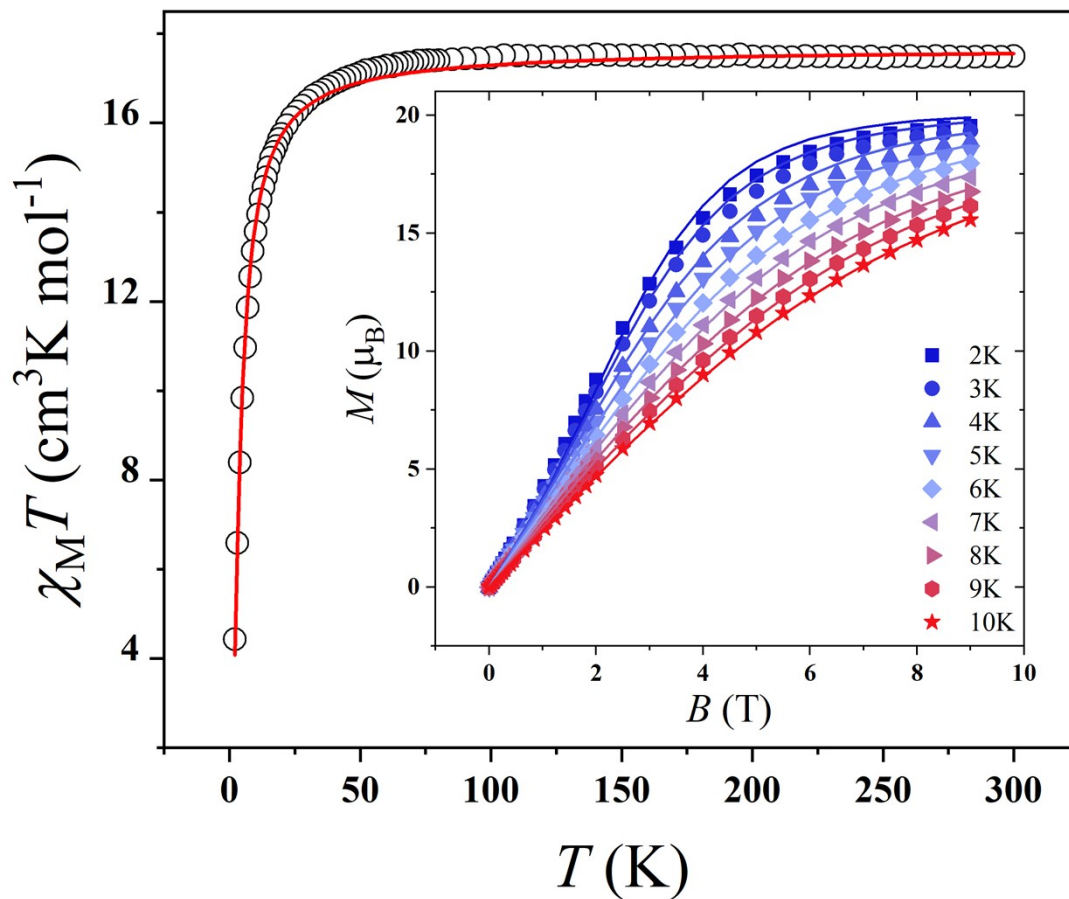
3. Magnetic Properties

Fig. S9. Best fit of the experimental χT product vs. T and M vs, B data for **1** using an anisotropic spin-Hamiltonian. The solid lines represent the best fit of the experimental data affording J_1 = -0.18 cm^{-1}, J_2 = +0.053 cm^{-1} and $|D|$ = 0.05 cm^{-1}, with g = 2.01 and zJ = +7.22 x 10^{-3} cm^{-1}.
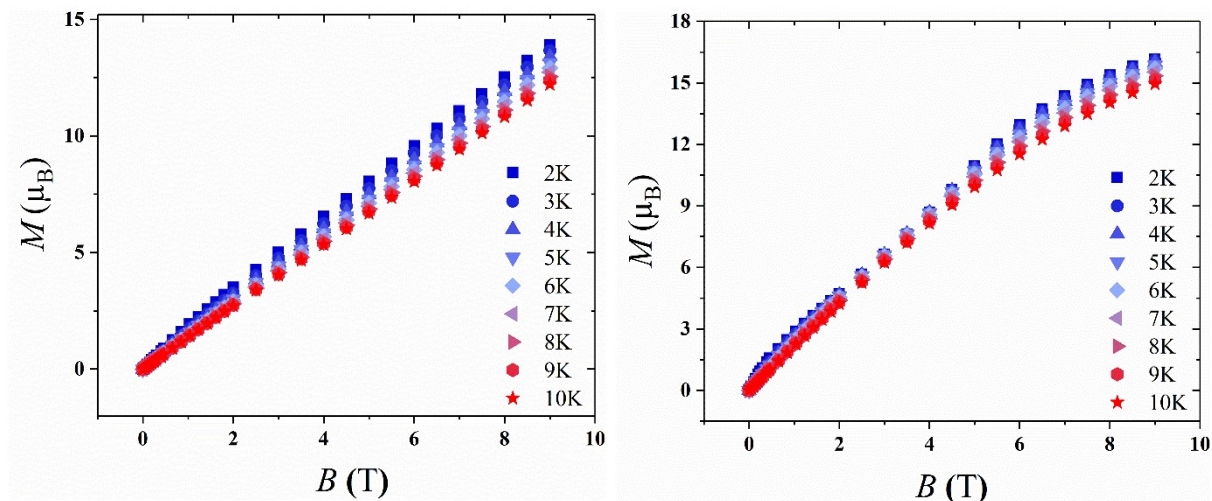
Fig. S10. Magnetisation (*M*) versus field (*B*) data for **2** (left) and **3** (right) measured in the *T* = 2-300 K and *B* = 0.5-9.0 T ranges, respectively.
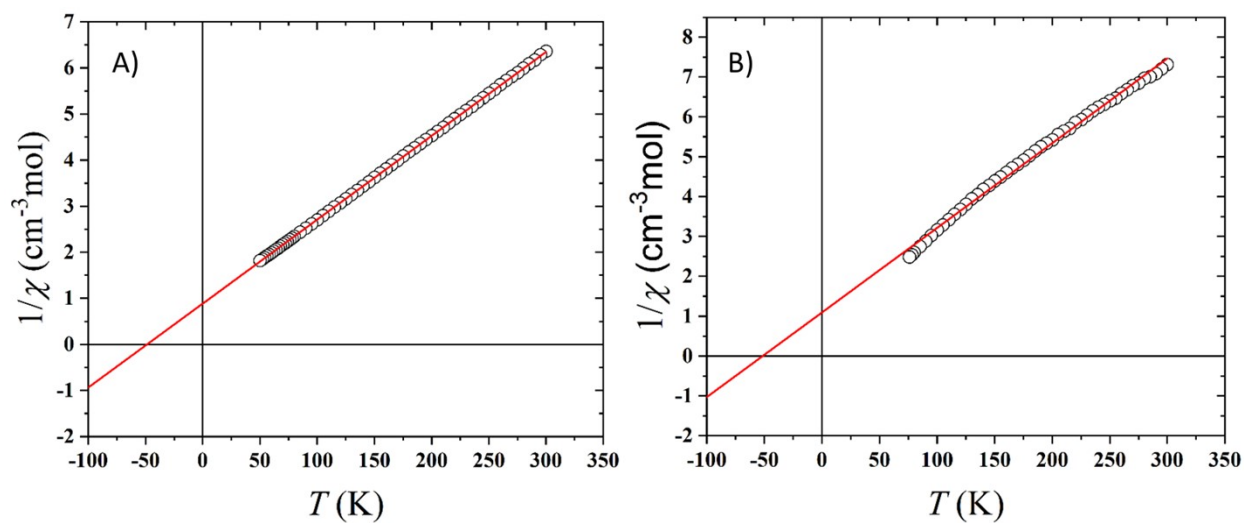

Fig. S11. Plot of 1/χ versus *T* for compounds **2** (A) and **3**(B). The solid red line is a fit of the Curie-Weiss law. See main text for details.
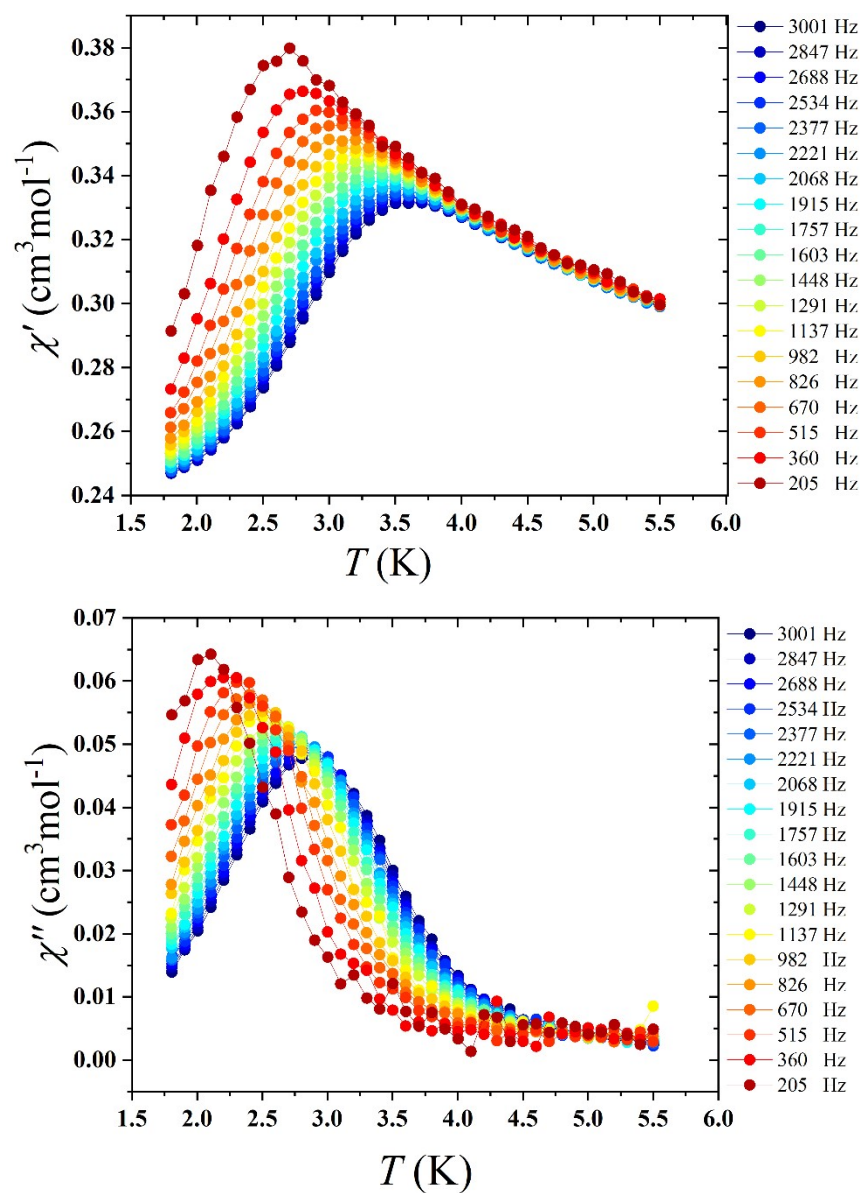
Fig. S12 Temperature dependence of the in-phase, χ' (upper), and out-of-phase, χ'' (lower), ac susceptibility data in zero dc field for compound **3** with ac frequencies in the range 205–3001 Hz.
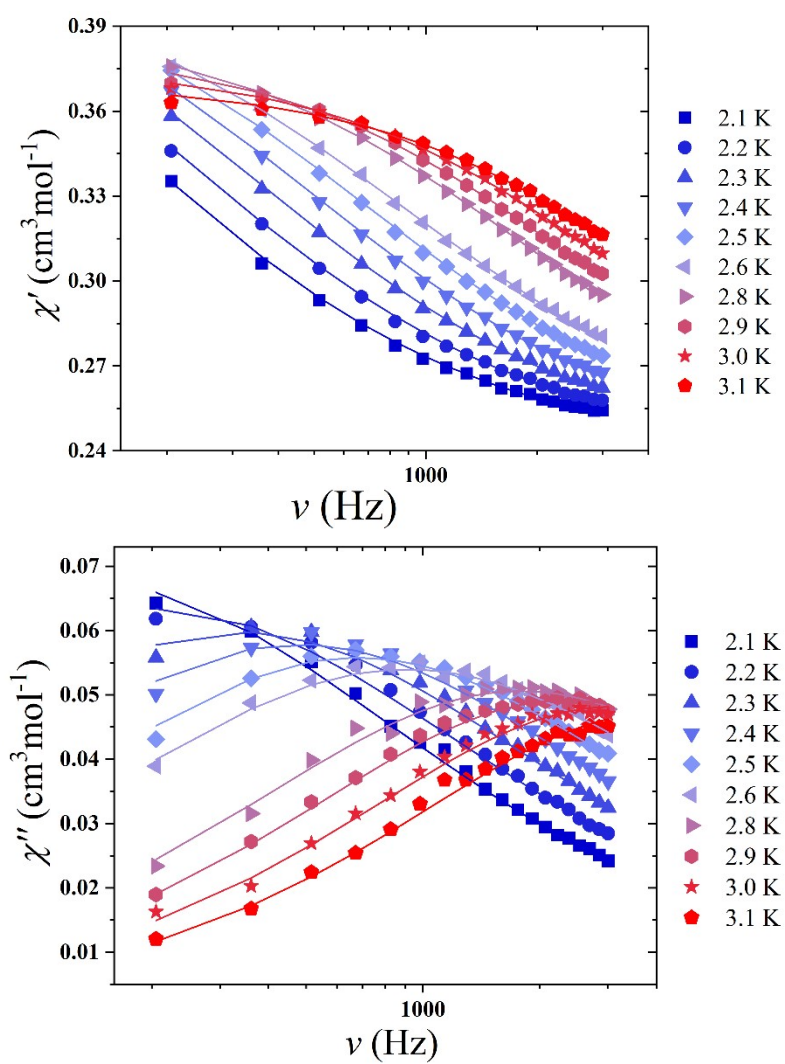
Fig. S13 Frequency dependence of the in-phase, χ' (upper), and out-of-phase, χ'' (lower), ac susceptibility for compound **3** in zero dc field. The solid lines correspond to the best fit to the generalised Debye law.
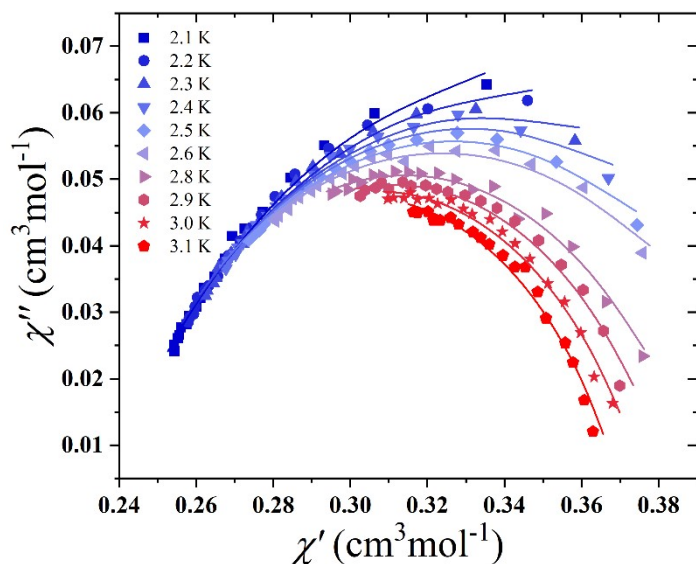
Fig. S14 χ″ vs χ′ plot of the ac magnetic susceptibility data of **3** in zero dc field. The solid lines correspond to the best fit of the Debye law.
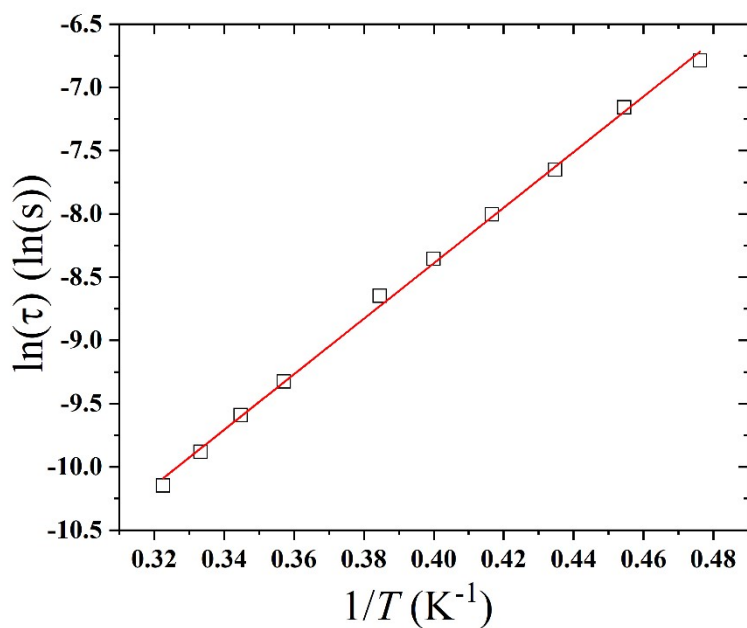

Fig. S15 Plot of the relaxation time τ (logarithmic scale) versus T^{-1} for compound **3**. The solid red line represents the best fit to the Arrhenius law, with U_{eff} = 22 K and τ_0 = 3.5 x 10^{-8} s.